Electronic Supplementary Material (ESI) for Energy & Environmental Science.

Electronic Supplementary Information for

Ampere-level CO_2 reduction to multicarbon products over a copper gas penetration electrode†

Chang Zhu,[ab] Yanfang Song,[ab] Xiao Dong,[a] Guihua Li,[ab] Aohui Chen,[ac] Wei Chen,*[ab] Gangfeng Wu,[ab] Shoujie Li,[ac] Wei Wei,*[abc] Yuhan Sun*[abc]

[a] CAS Key Laboratory of Low-Carbon Conversion Science and Engineering, Shanghai Advanced Research Institute, Chinese Academy of Sciences, Shanghai 201210, P.R. China
[b] University of Chinese Academy of Sciences, Beijing 100049, P.R. China
[c] School of Physical Science and Technology, ShanghaiTech University, Shanghai 201210, P.R. China
* E-mail: chenw@sari.ac.cn, weiwei@sari.ac.cn, sunyh@sari.ac.cn

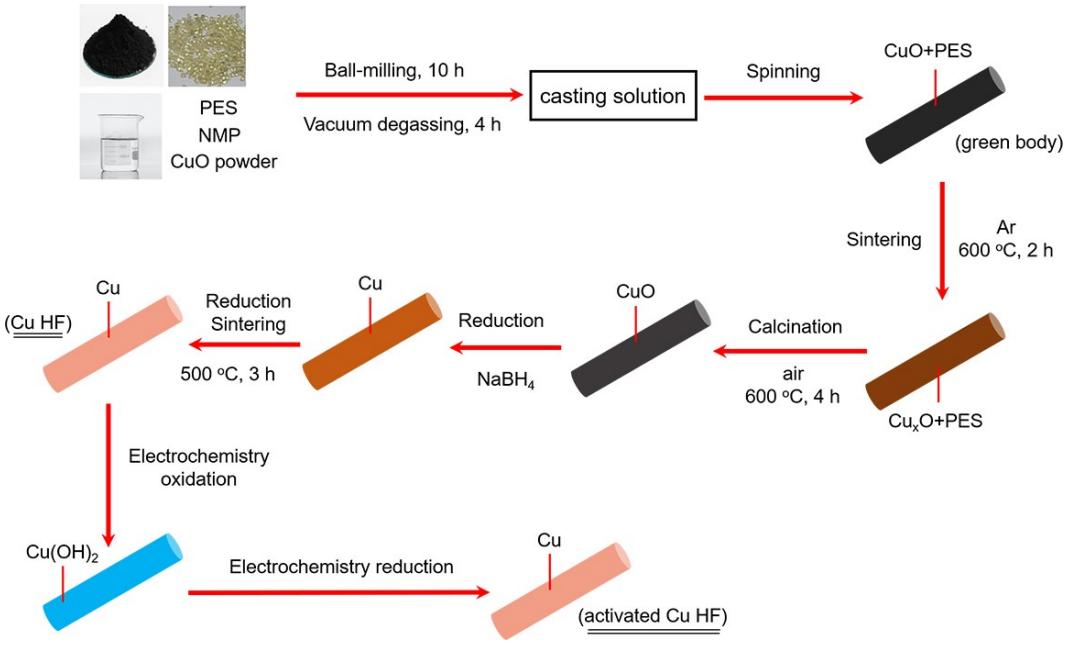

Fig. S1 Schematic illustration showing the general procedures for the fabrications of Cu HF and activated Cu HF.

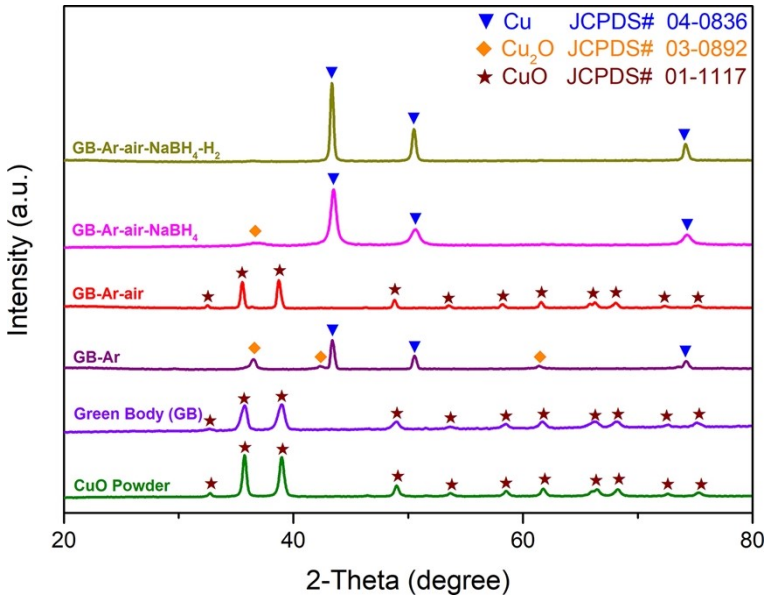

Fig. S2 XRD patterns of CuO powder (Olive), green body with shaped CuO and PES mixtures (Violet), green body sintered by Ar (Purple), CuO green body obtained by calcinating at 600 °C in the air (Red), Cu green body was obtained by reduction in $NaBH_4$ solution (Magenta), and Cu HF obtained by sintered in 5% H_2 (Ar balance) (Dark Yellow).

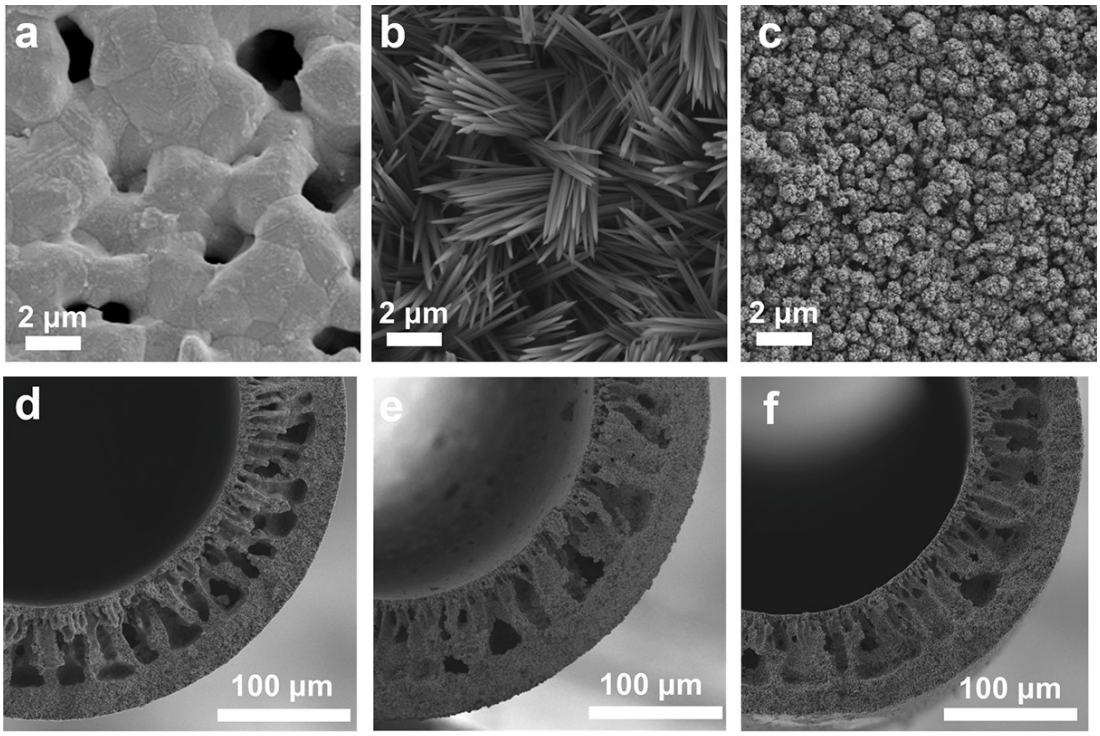

Fig. S3 SEM images of outer surface and cross-section of (a), (d) Cu HF, (b), (e) electrooxidated Cu HF, and (c), (f) activated Cu HF.

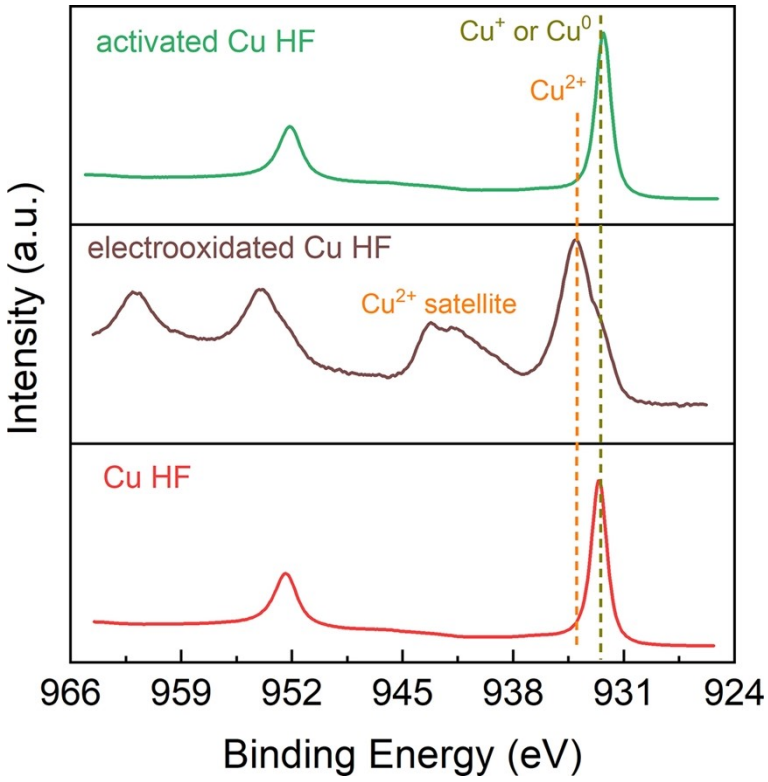

Fig. S4 Cu 2p XPS spectra of Cu HF, electrooxidated Cu HF and activated Cu HF.

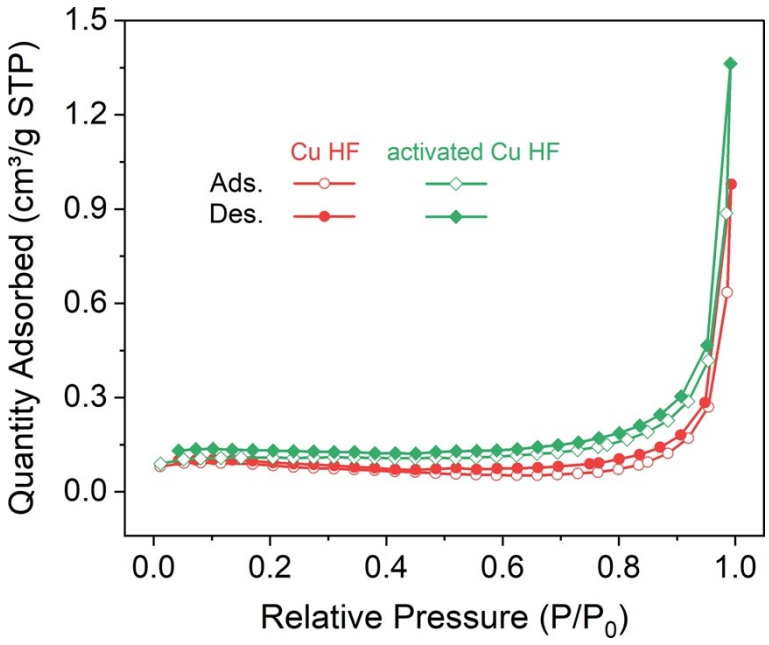

Fig. S5 N_2 adsorption-desorption isotherms of the Cu HF and activated Cu HF.

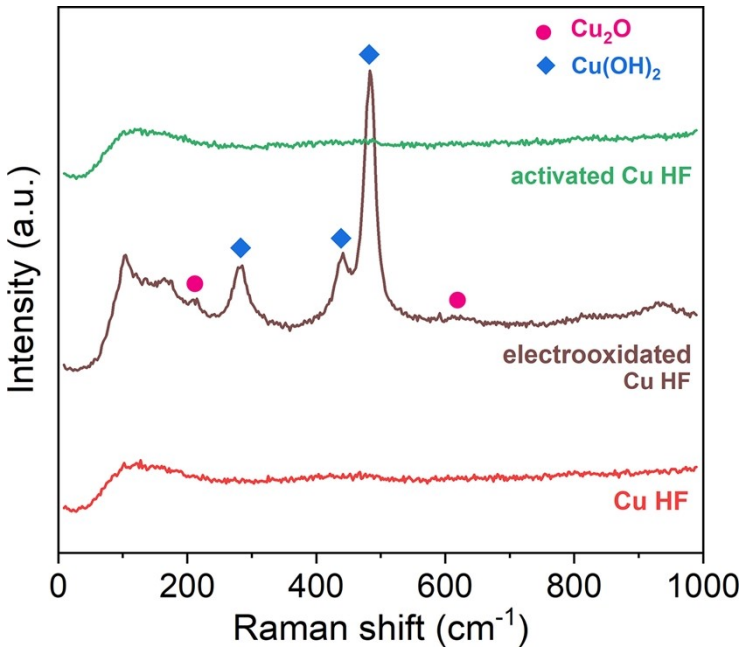

Fig. S6 Raman spectra of Cu HF, electrooxidated Cu HF and activated Cu HF.

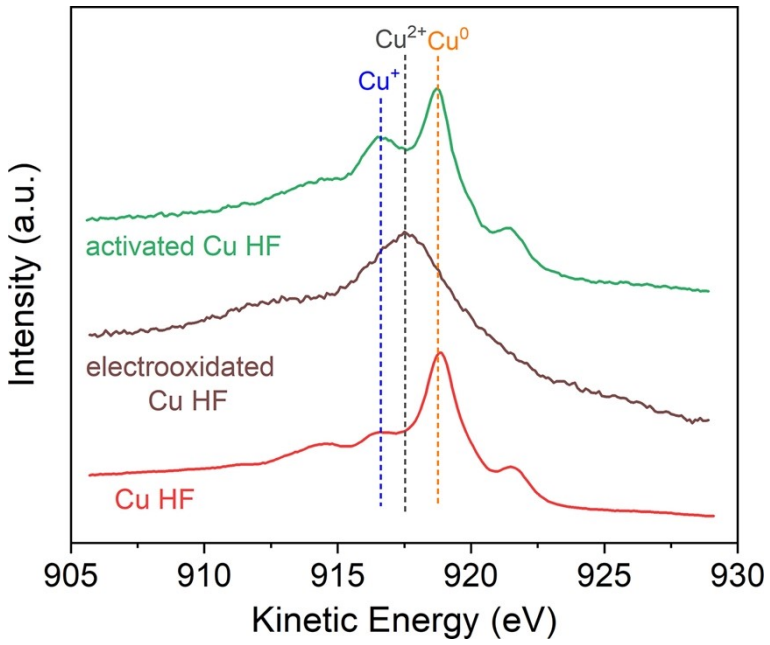

Fig. S7 Cu LMM Auger spectra of Cu HF, electrooxidated Cu HF and activated Cu HF.

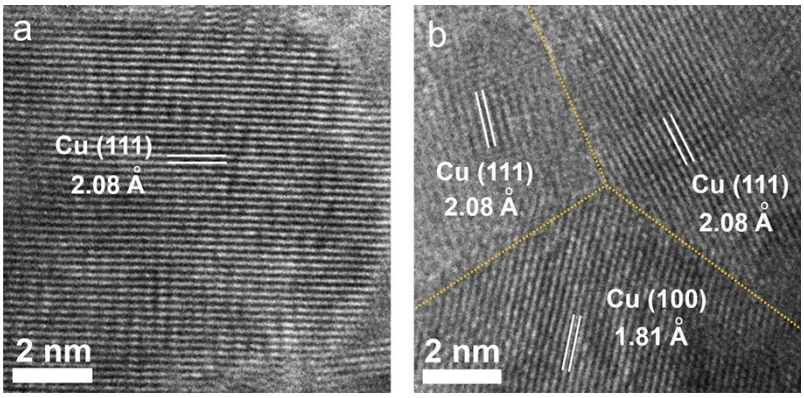

Fig. S8 HRTEM images of (a) Cu HF, and (b) activated Cu HF.

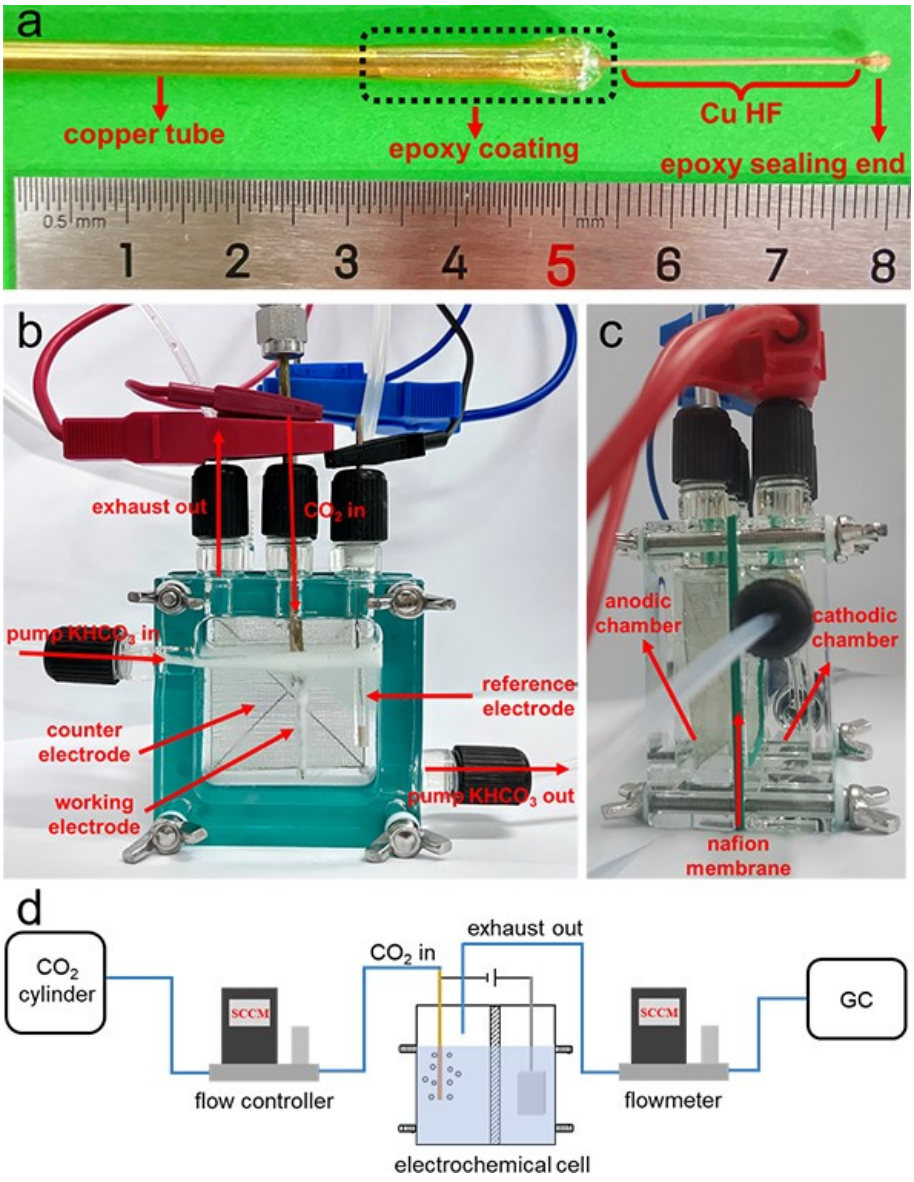

Fig. S9 Optical images of the (a) Cu HF electrode, (b) side view of the gas-tight two-compartment electrolysis cell, (c) cross-section view of the electrolysis cell, and (d) the schematic illustration of the electrolysis system for CO_2 electroreduction.

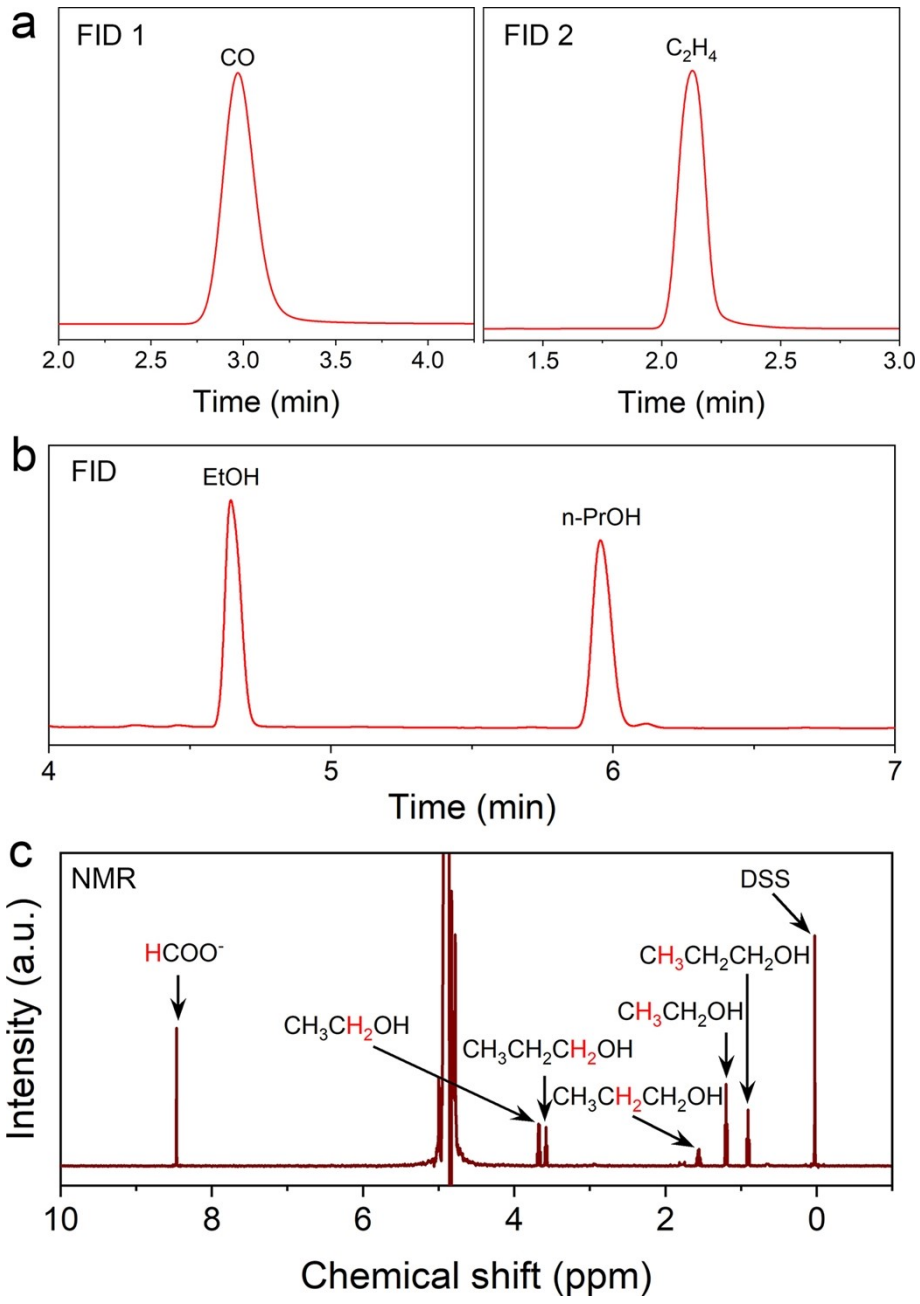

Fig. S10 (a) Gas chromatogram (FID channel) of the gas products during the eCO_2RR on activated Cu HF. (b) Off-line Gas chromatogram (FID channel) of alcohols used for detection after eCO_2RR on activated Cu HF. (C) Representative ^1H NMR spectrum of the catholyte after eCO_2RR on activated Cu HF.

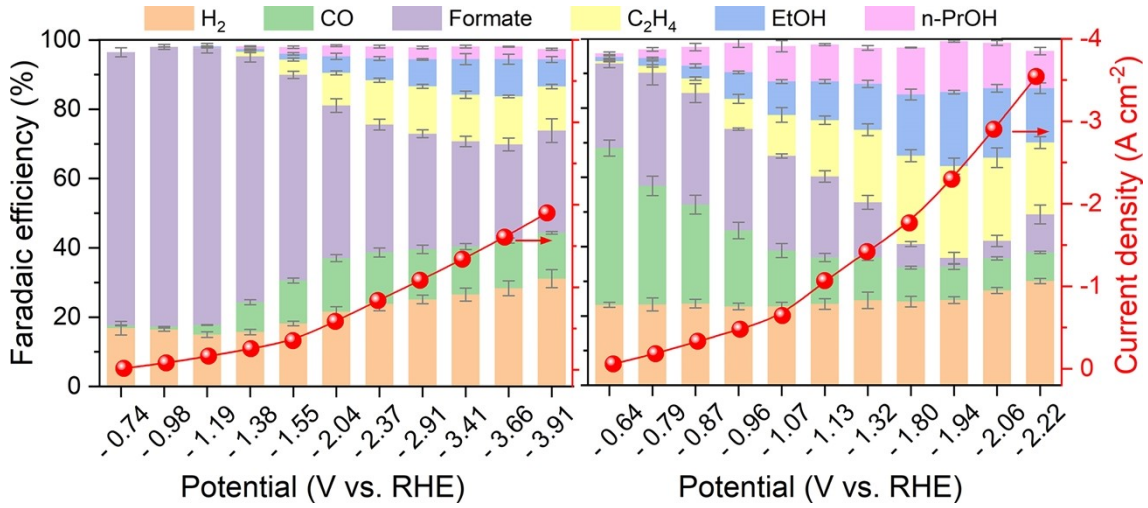

Fig. S11 Full product distributions and total current densities of Cu HF (left) and activated Cu HF (right) at different applied potentials.

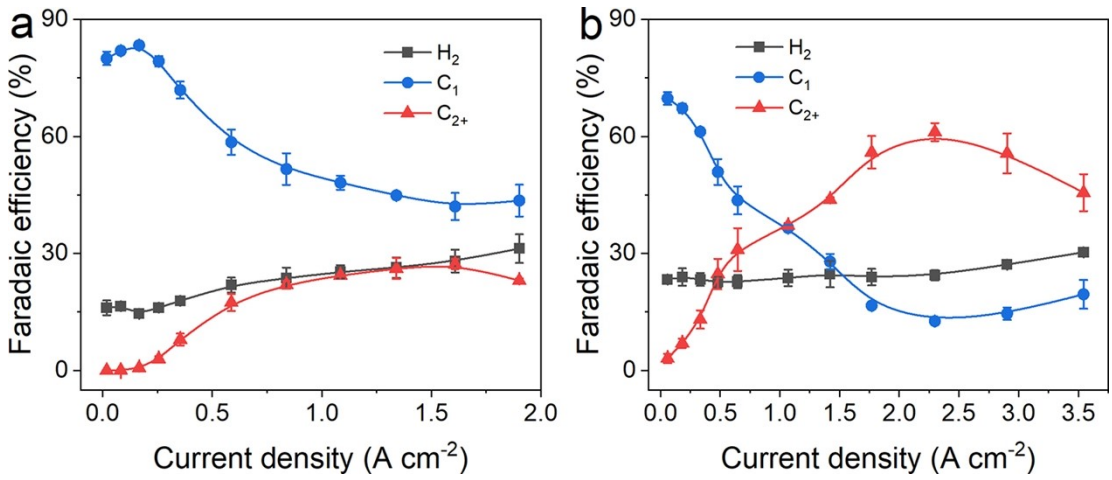

Fig. S12 Faradaic efficiency of H_2, C_1, and C_{2+} products of (a) Cu HF and (b) activated Cu HF at different current densities.

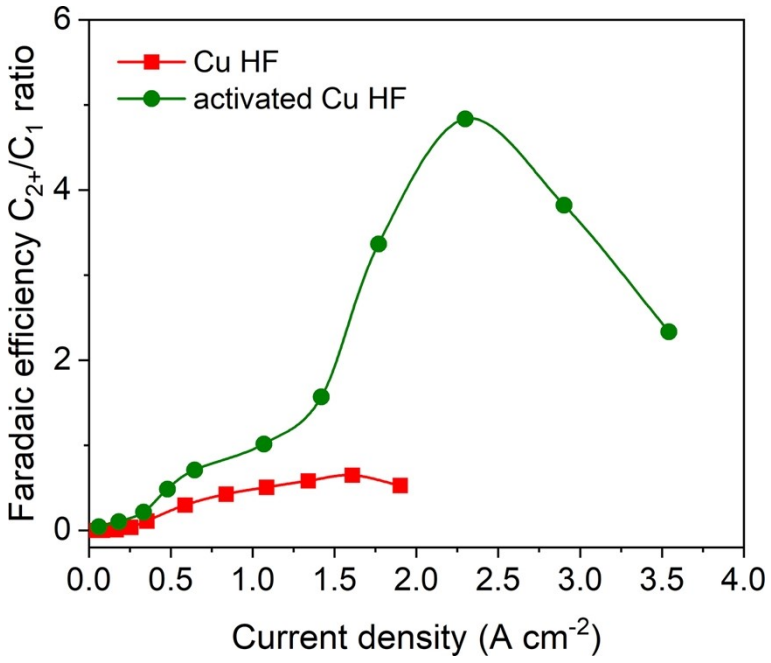

Fig. S13 C_{2+}/C_1 ratio at different current densities over Cu HF and activated Cu HF.

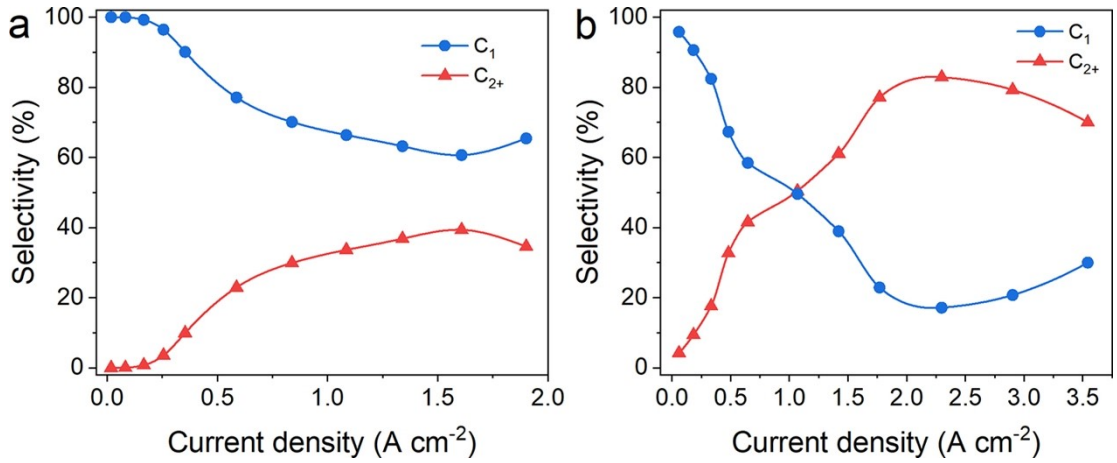

Fig. S14 Conversion efficiency of CO_2 to C_1 and C_{2+} products at different current densities of (a) Cu HF, and (b) activated Cu HF.

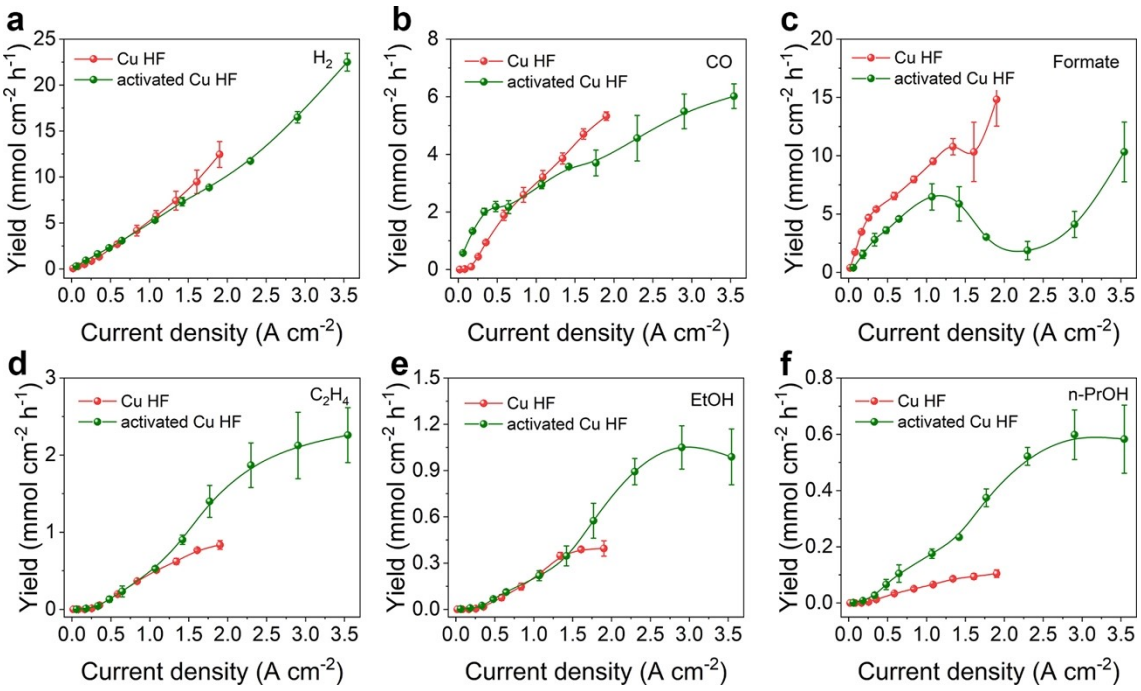

Fig. S15 Yields of the products (a) H_2, (b) CO, (c) formate, (d) C_2H_4, (e) EtOH, and (f) n-PrOH over the Cu HF and activated Cu HF electrodes.

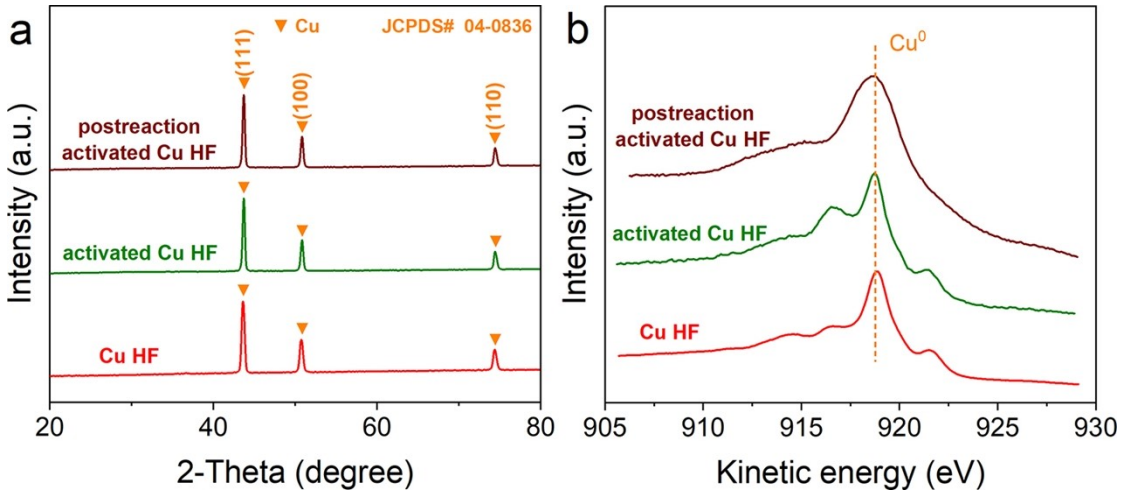

Fig. S16 The XRD patterns (a) and Cu LMM Auger spectra (b) of Cu HF (red), activated Cu HF (green), and postreaction activated Cu HF (wine).

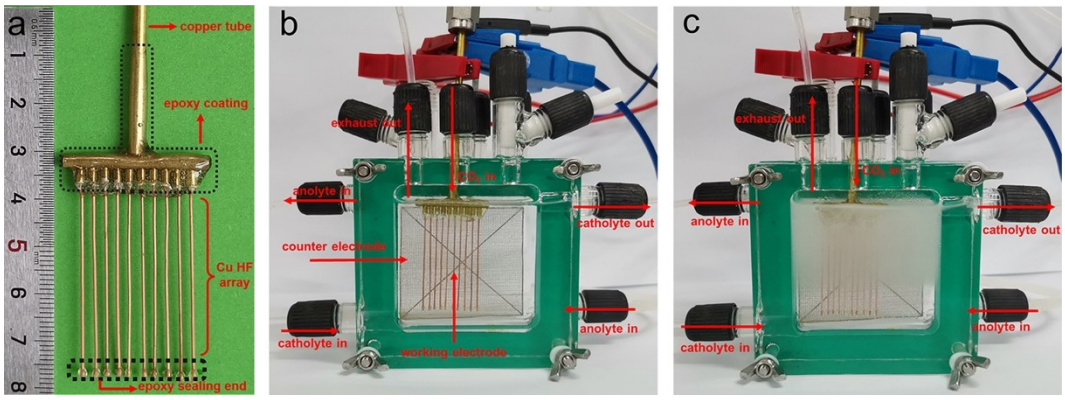

Fig. S17 Optical images of the (a) 10-tube activated Cu HF array, (b) side view of the gas-tight two-compartment electrolysis cell, and (c) the electrolysis cell during CO_2 electroreduction.

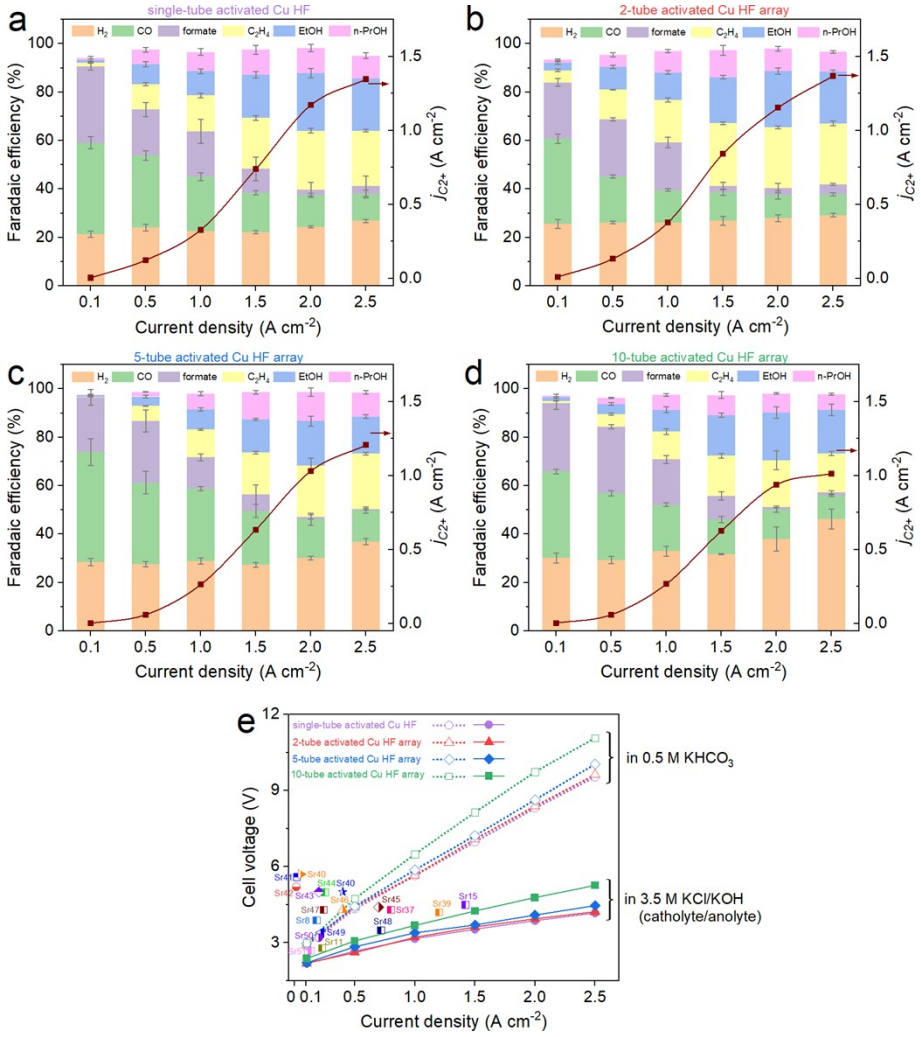

Fig. S18 Full product distributions and C_{2+} partial current densities at different current densities in 0.5 M $KHCO_3$ in the 2-electrode systems using (a) single-tube activated Cu HF, (b) 2-tube activated Cu HF array, (c) 5-tube activated Cu HF array, and (d) 10-tube activated Cu HF array. (e) Cell voltages at different current densities in 0.5 M $KHCO_3$ and 3.5 M KCl (as catholyte, KOH as anolyte), respectively, and their overall comparison with other electrocatalyst 2-electrode systems. All comparison data points are from the references summarized in Table S5, and the key data points are referred to the corresponding Supplementary references Srx, where x represents the Supplementary reference number.

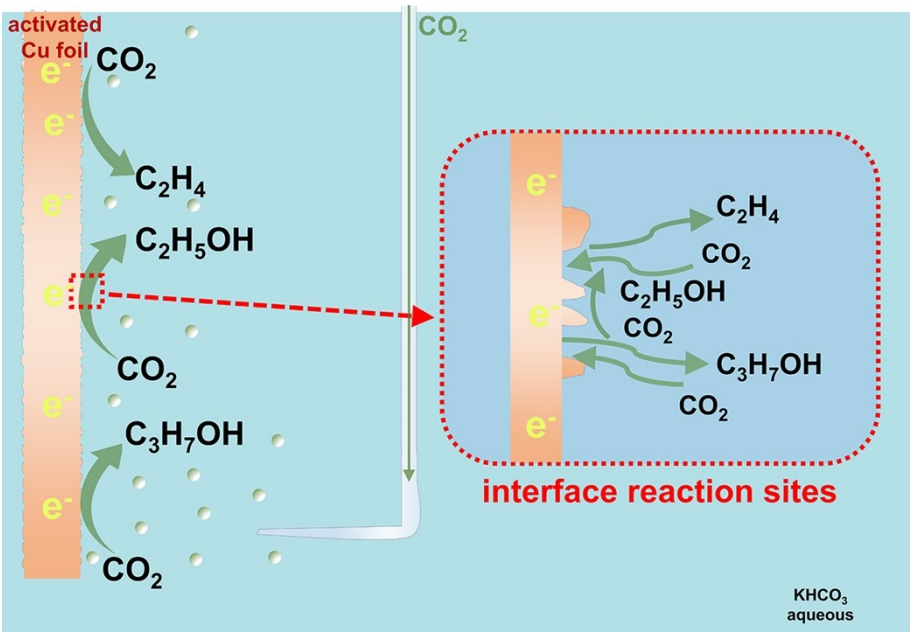

Fig. S19 Schematic illustrations showing the processes of CO_2 electroreduction over activated Cu foil.

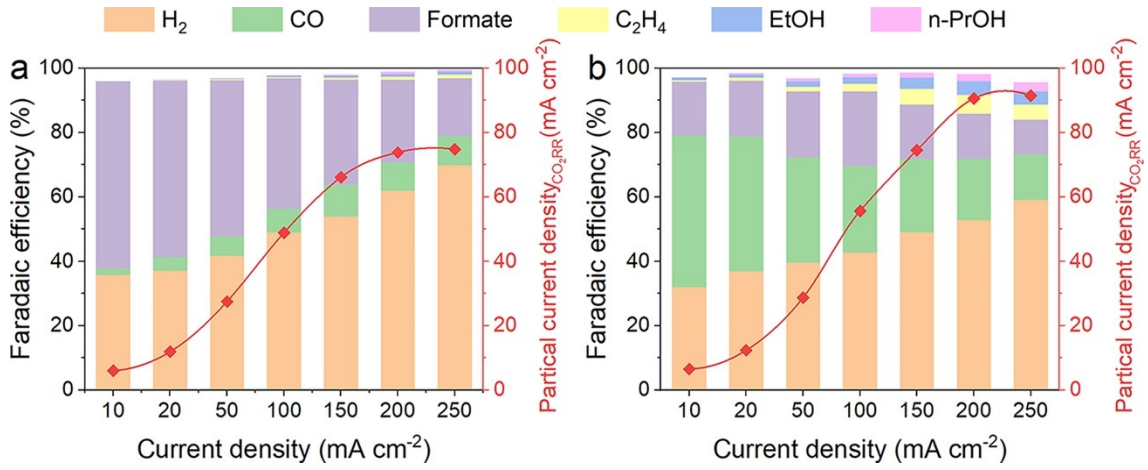

Fig. S20 Full product distributions and CO_2RR partial current density at different current densities of (a) Cu HF with non-penetration mode and (b) activated Cu HF with non-penetration mode.

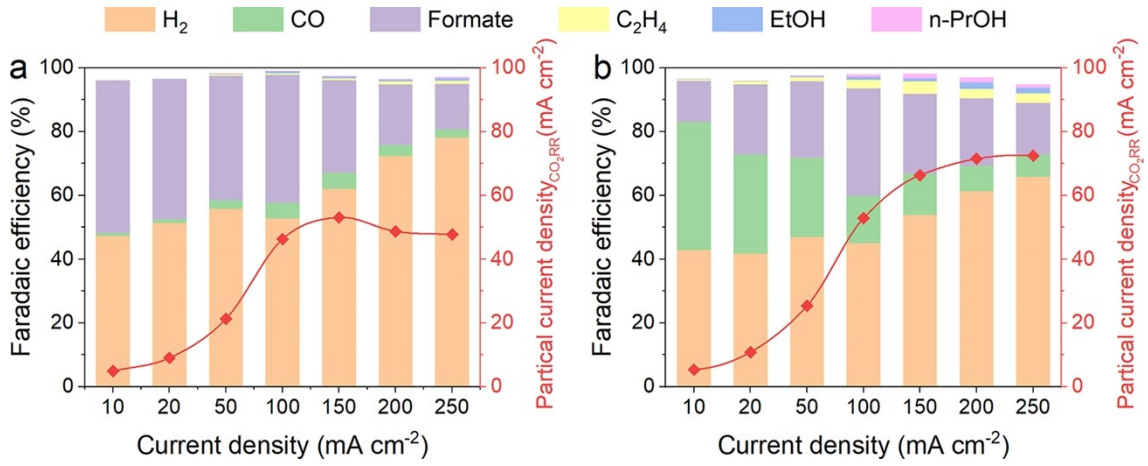

Fig. S21 Full product distributions and CO_2RR partial current density at different current densities of (a) Cu foil and (b) activated Cu foil.

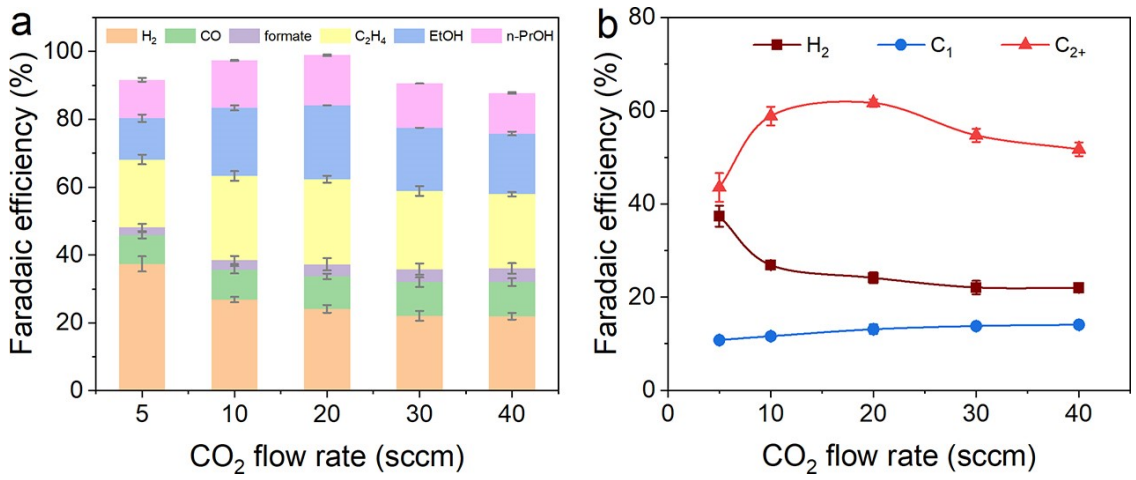

Fig. S22 (a) Full product distributions and (b) H_2, C_1, and C_{2+} products of activated Cu HF at 2.0 A cm^{-2} with different CO_2 flow rates.

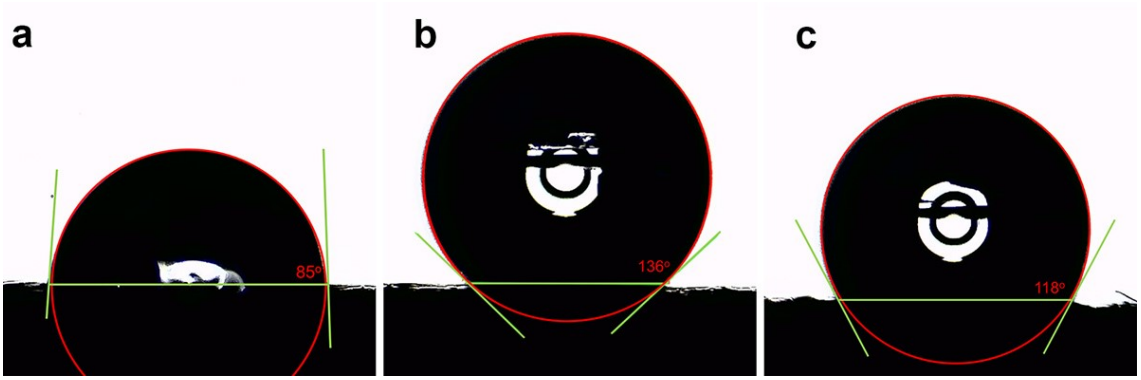

Fig. S23 The contact angles on the surfaces of (a) Cu HF, (b) electrooxidated Cu HF, and (c) activated Cu HF were tested.

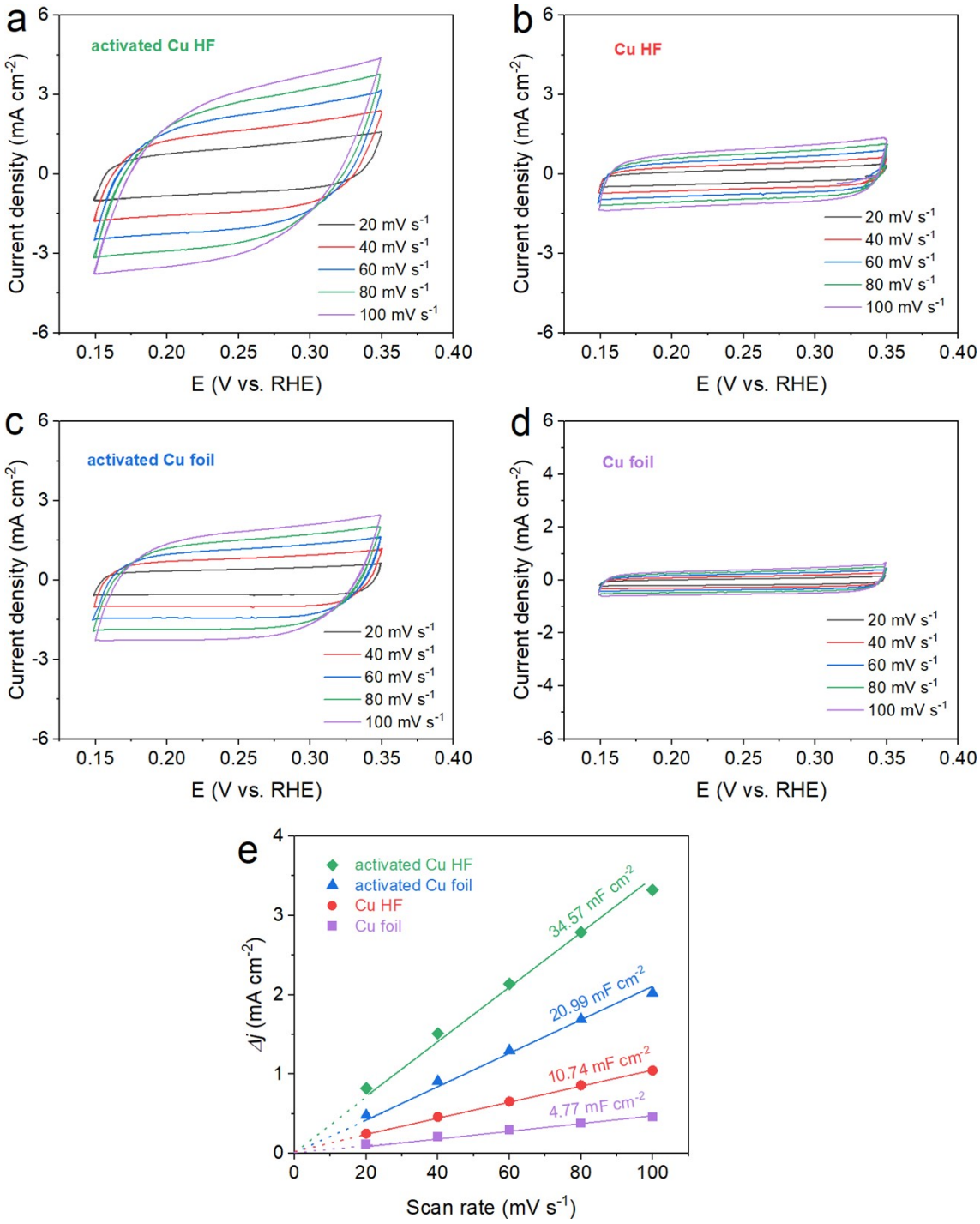

Fig. S24 Cyclic voltammetry curves of (a) activated Cu HF, (b) Cu HF, (c) activated Cu foil, and (d) Cu foil in Ar-saturated 0.5 M $KHCO_3$. (e) The plot of current density against the scan rates.

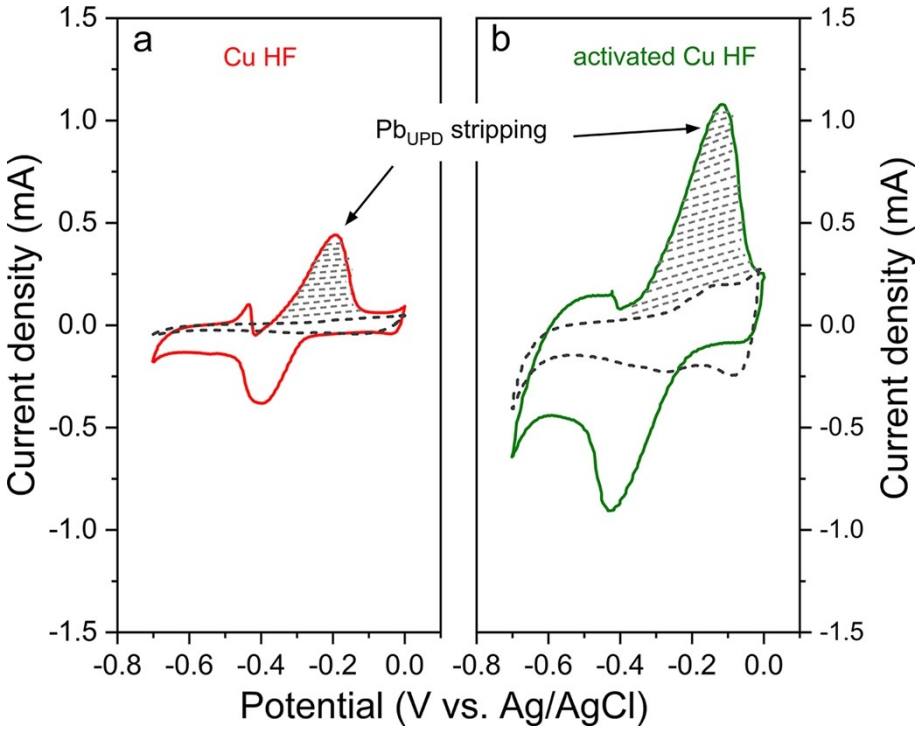

Fig. S25 Experiments of underpotential deposition of Pb^{2+} of (a) Cu HF and (b) activated Cu HF in two electrolytes: 1.0 mM $PbCl_2$ + 0.01 M $HClO_4$ (solid) and 0.01 M $HClO_4$ only (dashed). A cathodic peak observed ca. -0.38 V vs. Ag/AgCl corresponds to Pb UPD on Cu, and the anodic peak ca. -0.19 V corresponds to stripping of the Pb UPD monolayer layer. The charge density associated with Pb UPD stripping of 350 μC cm^{-2} was reported in the previous literature.[1]

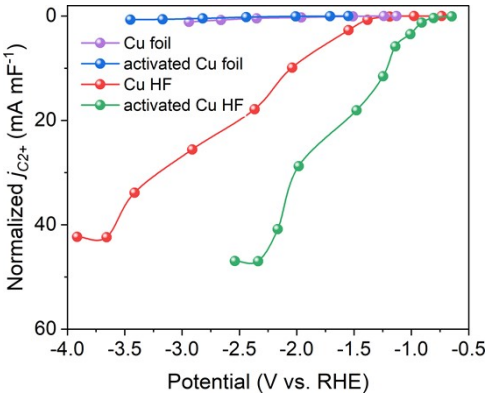

Fig. S26 ECSA-normalized partial current density of total C_{2+} products over Cu foil, activated Cu foil, Cu HF, and activated Cu HF.

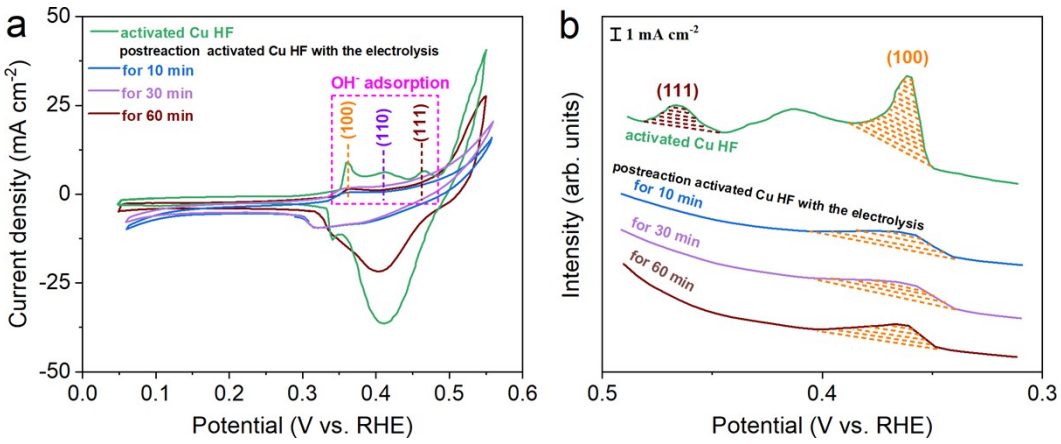

Fig. S27 (a) Voltammogram curves collected in 1 M KOH at room temperature with a sweep rate of 50 mV s^{-1}, and (b) OH^- adsorption profiles of activated Cu HF after the electrolysis for 10, 30, and 60 min, respectively.

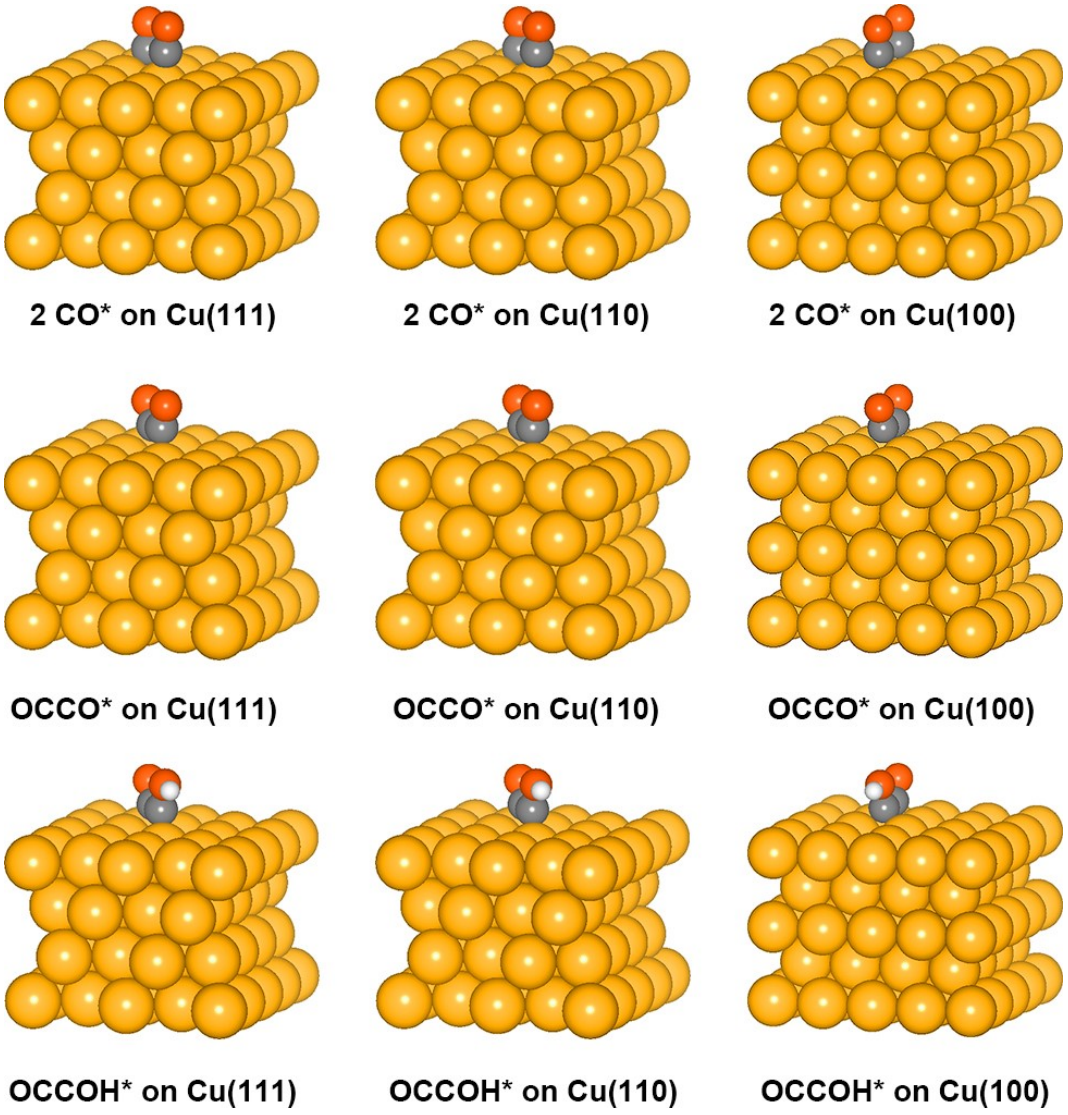

Fig. S28 Optimized surface slabs with adsorbed 2CO*, OCCO*, and OCCOH* on Cu (100), Cu (110), and Cu (111).

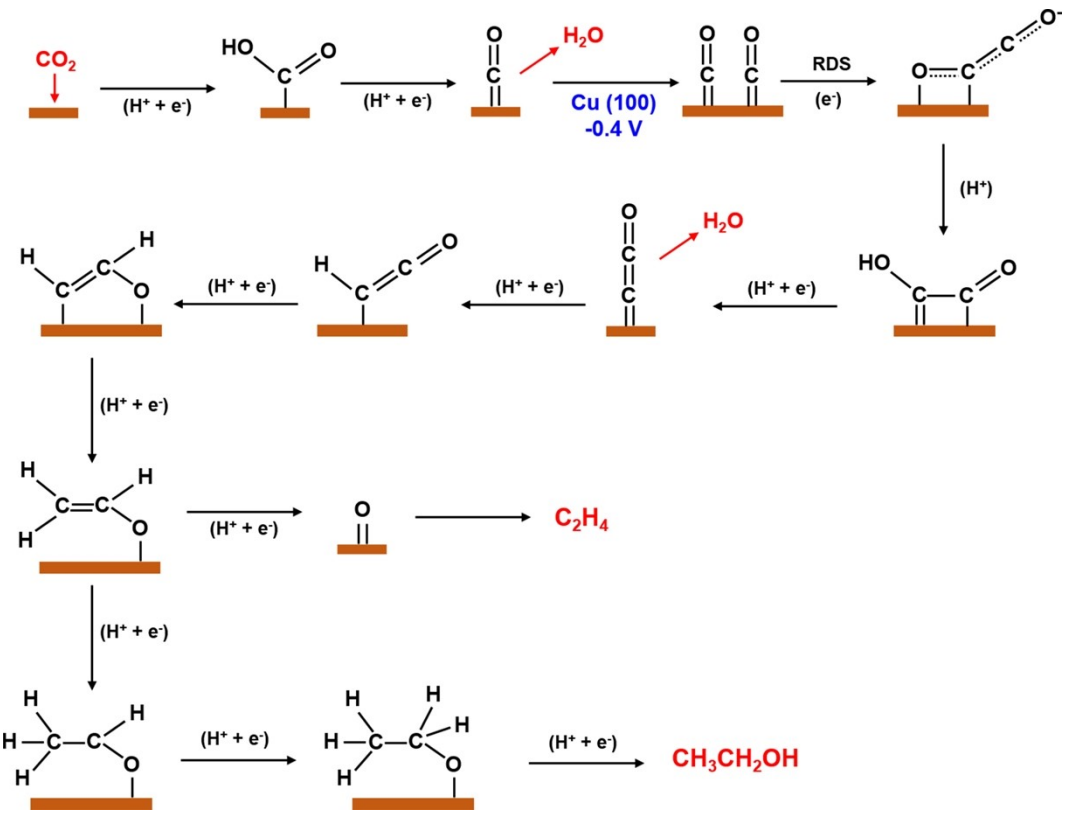

Fig. S29 Possible reaction pathways for the electrocatalytic reduction of CO_2 to C_2 products. Species in black are adsorbates, while those in red are reactants or products in solution. Potentials are reported versus RHE, while RDS indicates rate-determining steps and ($H^+ + e^-$) indicates steps in which either concerted or separated proton-electron transfer takes place.[2]

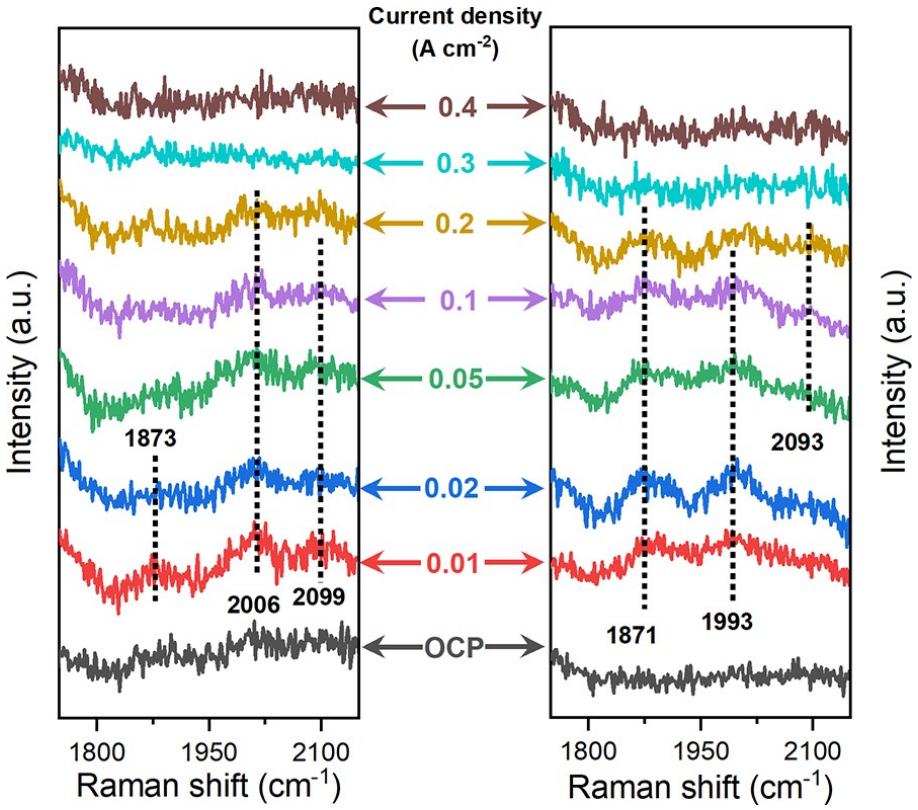

Fig. S30 In situ Raman spectra of Cu HF (left) and activated Cu HF (right) from 0.01 to 0.4 A cm^{-2} in CO_2-saturated 0.5 M $KHCO_3$ solution. All indicated peaks are assigned to the C≡O stretching mode.

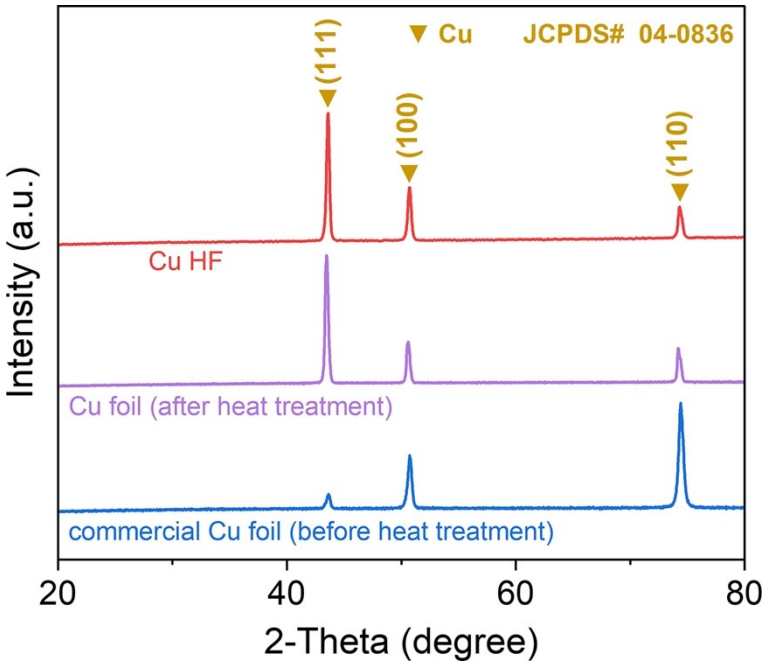

Fig. S31 XRD patterns of Cu HF, Cu foil (obtained from redox heat treatment) and commercial Cu foil.

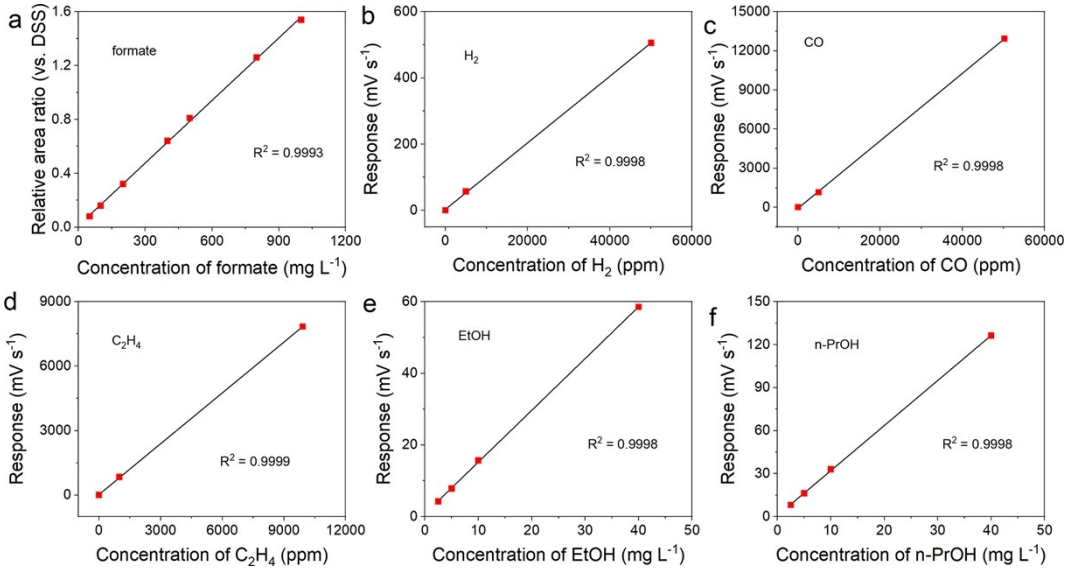

Fig. S32 Standard correlation curves and the corresponding linear correlation coefficients of all products. (a) formate detected by NMR, and (b) H_2, (c) CO, (d) C_2H_4, (e) EtOH, and (f) n-PrOH detected by GC.

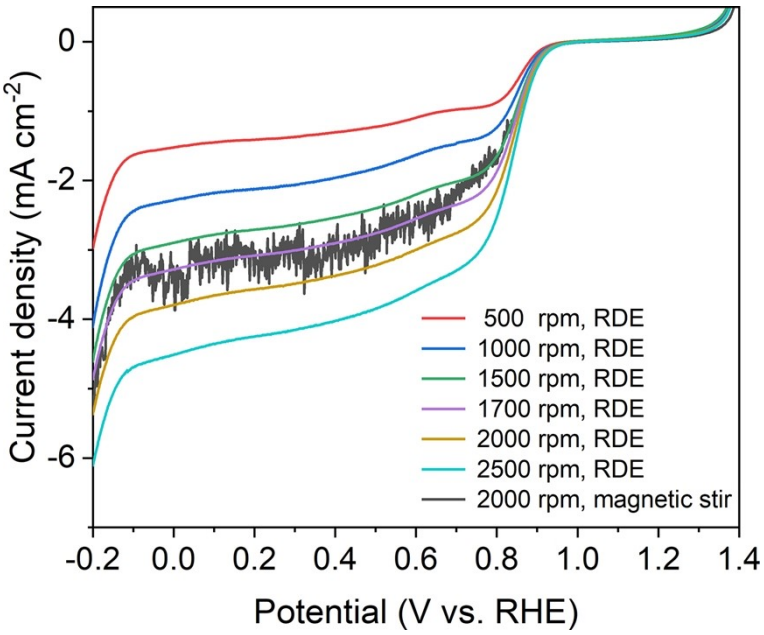

Fig. S33 LSV curves were measured at different rotation rates and magnetic stirrer with a speed of 2000 rpm.

Table S1 The pore structure parameters of Cu HF and activated Cu HF were obtained by N_2 sorption isotherm and mercury intrusion porosimetry, respectively.

Method	Parameters	Cu HF	activated Cu HF
N_2 sorption measurement	Surface Area ($m^2\ g^{-1}$)	0.3775	0.4194
	Pore Volume ($cm^3\ g^{-1}$)	0.000621	0.000398
	Calculated porosity (%)	0.28	0.18
Mercury intrusion porosimetry	Calculated porosity (%)	68	59

Table S2 Comparisons of the electrocatalytic performance for CO_2 to C_{2+} products at different applied potentials in different electrolytes.

Potential (V vs. RHE)	Electrolyte	Product	FE (%)	j_{C2+} (mA cm^{-2})	j_{total} (A cm^{-2})	Ref.
-1.07	0.5 M $KHCO_3$	C_{2+}	34.9	225	0.6	This work
-1.32	0.5 M $KHCO_3$	C_{2+}	44.2	628	1.4	
-1.94	0.5 M $KHCO_3$	C_{2+}	62.8	1442	2.3	
-0.70	3.5 M KCl*	C_{2+}	27.9	139	0.5	This work
-0.84	3.5 M KCl	C_{2+}	47.5	475	1.0	
-0.95	3.5 M KCl	C_{2+}	64.8	1296	2.0	
-1.00	0.5 M $KHCO_3$	C_2H_4	45.0	45	0.1	3
-1.20	0.5 M $KHCO_3$	C_{2+}	57.3	41	0.07	4
-1.40	0.5 M $KHCO_3$	C_{2+}	36.0	32	0.09	
-1.00	0.5 M $KHCO_3$	C_{2+}	51.0	17	0.03	5
-1.00	0.5 M $KHCO_3$	C_2H_4	11.3	2	0.02	6
-1.02	0.5 M $KHCO_3$	C_2H_4	36.0	20	0.06	7
-1.31	0.5 M $KHCO_3$	C_2H_4	10.0	10	0.10	
-0.83	1.0 M $KHCO_3$	C_2H_4	72.0	232	0.3	8
-1.20	0.1 M $KHCO_3$	C_{2+}	52.0	31	0.06	9
-1.39	0.1 M $KHCO_3$	C_{2+}	47.5	46	0.1	
-0.98	0.1 M $KHCO_3$	C_{2+}	59.0	23	0.04	10
-1.19	0.1 M $KHCO_3$	C_{2+}	45.0	24	0.05	
-0.89	0.75 M KOH	C_{2+}	80.0	1280	1.6	11
-1.00	0.75 M KOH	C_{2+}	58.0	1160	2.0	
-0.97	1.0 M KOH	C_{2+}	90.0	390	0.4	12
-1.00	1.0 M KOH	C_{2+}	66.1	591	0.9	13
-1.15	1.0 M KOH	C_{2+}	73.7	909	1.2	14
-1.21	1.0 M KOH	C_{2+}	57.0	820	1.4	
-0.55	3.5 M KOH	C_2H_4	63.0	473	0.8	15
-0.91	7.0 M KOH	C_{2+}	78.2	1212	1.6	16
-1.10	0.1 M KCl	C_{2+}	79.0	55	0.7	17
-0.80	0.1 M KCl	EtOH	43.0	0.2	0.0005	18
-1.20	0.1 M KCl	EtOH	18.0	1	0.006	
-1.20	0.1 M KCl	C_2H_4	45.2	8	0.02	19
-1.30	0.1 M KCl	C_2H_4	37.0	9	0.03	
-1.28	0.1 M KCl	C_2H_4	42.0	4.2	0.01	20
-1.58	0.1 M KCl	C_2H_4	20.0	6.6	0.03	
-1.20	0.2 M KCl	C_{2+}	49.4	1.0	0.002	21
-1.40	0.2 M KCl	C_{2+}	33.0	1.0	0.003	
-0.81	0.5 M KCl	C_2H_4	84.5	169	0.2	22
-1.24	2.0 M KCl	C_{2+}	57.9	92	0.2	23
-1.20	3.0 M KCl	C_{2+}	82.7	97	0.1	

* 3.5 M KCl as catholyte, and 3.5 M KOH as anolyte.

Table S3 The amount of dissolved Cu in the electrolyte during eCO_2RR over activated Cu HF is quantified by ICP-OES.

Reaction time	Dissolved Cu
0-10 min (OCP)	N.D.*
0-10 min (0.1 A cm^{-2})	N.D.
0-10 min (1.0 A cm^{-2})	N.D.
1.0 h (stability test)	N.D.
10 h (stability test)	N.D.
20 h (stability test)	N.D.
30 h (stability test)	N.D.

*N.D. — not detected

Table S4 Electrocatalytic performances for CO_2 to C_{2+} products over the prominent catalysts reported with different electrode types.

Catalyst	Potential (V vs. RHE)	Electrode Type	Electrolyte	FE_{C2+} (%)	j_{C2+} (mA cm^{-2})	Ref.
activated Cu HF	-1.07	Hollow-fiber GPEs*	0.5 M $KHCO_3$	34.86	225	This work
activated Cu HF	-1.32	Hollow-fiber GPEs	0.5 M $KHCO_3$	44.18	628	
activated Cu HF	-1.94	Hollow-fiber GPEs	0.5 M $KHCO_3$	62.75	1442	
activated Cu HF	-0.70	Hollow-fiber GPEs	3.5 M KCl	27.9	139	This work
activated Cu HF	-0.84	Hollow-fiber GPEs	3.5 M KCl	47.5	475	
activated Cu HF	-0.95	Hollow-fiber GPEs	3.5 M KCl	64.8	1296	
Cu_2O derived Cu	-0.99	Planar electrode**	0.1 M $KHCO_3$	48.7	12.18	24
Cu/CNS	-1.2	Planar electrode	0.1 M $KHCO_3$	63	1.26	25
Cu_4Zn	-1.05	Planar electrode	0.1 M $KHCO_3$	45.16	3.71	26
Plasma-Cu	-0.9	Planar electrode	0.1 M $KHCO_3$	60	13.81	27
Cu nanocubes	-1.1	Planar electrode	0.1 M $KHCO_3$	47.6	1.90	28
Au/Cu	-0.97	Planar electrode	0.1 M $KHCO_3$	22.7	1.86	29
(100) Cu NBs	-0.96	Planar electrode	0.25 M $KHCO_3$	60.5	41.14	30
B-doped Cu	-1.1	Planar electrode	0.1 M KCl	79	55.3	17
Cu NAs	-1.1	Planar electrode	0.1 M $KClO_4$	29	1.31	31
Cu foil	-0.83	Planar electrode	0.1 M $KHCO_3$ + 0.3 M KI	28	1.26	32
Cu-12	-0.83	Membrane-GDEs***	0.1 M $KHCO_3$	72	231.84	8
Dendritic Cu	-1.2	Membrane-GDEs	0.1 M $KHCO_3$	36	162	9
N-C-Cu	-0.68	Membrane-GDEs	1.0 M KOH	92.1	276.3	33
Cu_2S–Cu-V	-0.92	Membrane-GDEs	1.0 M KOH	32	126.08	34
F-Cu	-0.89	Membrane-GDEs	0.75 M KOH	80	1280	11
Cu_3Nx	-1.15	Membrane-GDEs	1.0 M KOH	81.7	307.19	35
$Cu(OH)_2$-D	-0.54	Membrane-GDEs	1.0 M KOH	87	217.5	10
Cu nanoparticle	-0.58	Membrane-GDEs	1.0 M KOH	46	197.8	36
Porous Cu	-0.67	Membrane-GDEs	1.0 M KOH	61.9	404.21	37
CuAg-wire	-0.7	Membrane-GDEs	1.0 M KOH	85	255	38
CIPH	-0.91	Membrane-GDEs	7.0 M KOH	78.2	1212	16
C/Cu/PTFE	-0.55	Membrane-GDEs	3.5 M KOH	63	472.5	15
Cu-CO_2-60	-0.69	Membrane-GDEs	8.0 M KOH	90	520.2	39
Cu nanoparticle	-0.85	Membrane-GDEs	10 M KOH	18	54	40
Cu/PFSA	-1.34	Membrane-GDEs	1 M H_3PO_4+3 M KCl	50	600	41

* Hollow-fiber GPEs — CO_2 forces penetration through the hollow fiber wall into the electrolyte and forces interaction with the active site.

** Planar electrode — Electrodes immersed in the electrolyte use CO_2 dissolved in the electrolyte as the reactant.

*** Membrane-GDEs — CO_2 diffuses through the membrane to the catalyst layer and reacts with CO_2 gas near the membrane electrode.

Table S5 Cell voltages of the prominent electrocatalysts reported with 2-electrode system.

Electrolyte	Product	Cell voltage (V)	j_{total} (A cm^{-2})	Ref.
CO_2+H_2O	C_2H_4	5.7	0.05	42
CO_2+H_2O	C_2H_4	5.0	0.40	
0.1 M $KHCO_3$	C_{2+}	5.6	0.015	43
0.3 M Bu_4NClO_4/PC	CO	5.2	0.013	44
0.1 M $CsHCO_3$	CO	5.0	0.20	45
CO_2+H_2O	C_{2+}	5.0	0.25	46
7 M KOH	C_{2+}	4.5	1.42	16
CO_2+H_2O	CH_4	4.4	0.70	47
1 M KOH	C_{2+}	4.3	0.40	48
7 M KOH	C_{2+}	4.3	0.80	39
0.01 M H_2SO_4	C_{2+}	4.3	0.24	49
1 M H_3PO_4+3 M KCl	C_{2+}	4.2	1.200	41
CO_2+H_2O	C_2H_4	3.9	0.18	8
1 M KOH	C_{2+}	3.5	0.72	50
0.5 M $NaHCO_3$	CO	3.4	0.22	51
0.5 M $KHCO_3$	CO	4.5	3.37	52
0.1 M $KHCO_3$	C_{2+}	3.4	0.50	53
0.5 M $KHCO_3$	C_2H_4	3.2	0.20	22
0.01 M H_2SO_4	C_{2+}	3.8	0.09	54
0.1 M H_2SO_4 + 0.4 M K_2SO_4	C_{2+}	3.2	0.20	55
2.5 M KOH	C_{2+}	2.8	0.23	11
CO_2+H_2O	CO	2.7	0.14	56

Table S6 Different theoretical limits ($j_{product,limit(gas)}$ and $j_{product,limit(sol)}$) and j_{CO2RR} values over activated Cu HF were obtained at different CO_2 flow rates.

j (A cm^{-2}) \ CO_2 flow rate (ml min^{-1})		5	10	20	30	40
theoretica $j_{product,limit(gas)}$ (A cm^{-2})	n=2	2.15	4.31	8.61	12.92	17.22
	n=6	6.46	12.92	25.84	38.76	51.68
theoretical $j_{product,limit(sol)}$ (A cm^{-2})	n=2	0.09	0.09	0.09	0.09	0.09
	n=6	0.26	0.26	0.26	0.26	0.26
experimental j_{CO2RR} (A cm^{-2})		1.09	1.41	1.49	1.37	1.32

All gas-phase CO_2 molecules input into the electrolysis cell were reduced with a 100% conversion rate, i.e., $j_{product,limit(gas)}$, and all CO_2 molecules dissolved in the electrolyte solution were reduced, i.e., $j_{product,limit(sol)}$.

The theoretical limits of C_{2+} products partial current density, i.e., $j_{C2+,lim(gas)}$ was calculated by the following Equation:

$$j_{limit(gas)} = (n \times F \times v_{CO_2})/(S_{HF} \times V_m)$$

where n is the number of moles of electrons transferred in the half-reaction. F is the Faraday constant, 96485 C mol^{-1}. S_{HF} is the electrode area, v_{CO2} is the flow rate of CO_2, and V_m is the gas mole volume (24.5 L mol^{-1} at 25 °C, 101.325 kPa).

Based on the semi-infinite diffusion model, the current density under the mass transport limit can be evaluated using the following equation:

$$j_{limit(sol)} = n \times F \times D \times c/\delta$$

where D is the diffusion coefficient of CO_2, 2 ×10^{-5} cm^2 s^{-1}. c represents the saturated bulk concentration of CO_2, and the solubility of CO_2 in the diluted aqueous electrolyte at 1atm is 34 mM. δ is the diffusion layer thickness for CO_2.

Table S7 Double-layer capacitance and Pb UPD results obtained by cyclic voltammetry.

Electrode	Double layer capacitance (mF cm^{-2})	Ratio of activated Cu HF/ Cu HF	Pb UPD (mC)	Ratio of activated Cu HF/ Cu HF
Cu HF	10.74	3.22	3.12	3.38
activated Cu HF	34.57		10.56	
Cu foil	4.77	/	/	/
activated Cu foil	20.99	/	/	/

Table S8 Adsorption energies of three intermediates (CO*, OCCO*, and OCCOH*) in CO_2 reduction on Cu(111), Cu(110), Cu(100). All energies are expressed in eV.

	Cu(111)	Cu(110)	Cu(100)
CO*	0 eV	0 eV	0 eV
OCCO*	1.14 eV	0.85 eV	0.74 eV
OCCOH*	1.00 eV	0.71 eV	0.49 eV

References

(1) L. Wang, S. Nitopi, A. B. Wong, J. L. Snider, A. C. Nielander, C. G. Morales-Guio, M. Orazov, D. C. Higgins, C. Hahn and T. F. Jaramillo, *Nat. Catal.*, 2019, **2**, 702-708.

(2) F. Calle-Vallejo and M. T. Koper, Angew. Chem., Int. Ed., 2013, **52**, 7282-7285.

(3) W. Zhang, C. Huang, Q. Xiao, L. Yu, L. Shuai, P. An, J. Zhang, M. Qiu, Z. Ren and Y. Yu, J. Am. Chem. Soc., 2020, **142**, 11417-11427.

(4) H. Wu, J. Li, K. Qi, Y. Zhang, E. Petit, W. Wang, V. Flaud, N. Onofrio, B. Rebiere, L. Huang, C. Salameh, L. Lajaunie, P. Miele and D. Voiry, Nat. Commun., 2021, **12**, 7210.

(5) Z. Lyu, S. Zhu, L. Xu, Z. Chen, Y. Zhang, M. Xie, T. Li, S. Zhou, J. Liu, M. Chi, M. Shao, M. Mavrikakis and Y. Xia, J. Am. Chem. Soc., 2021, **143**, 149-162.

(6) P. Shao, W. Zhou, Q. L. Hong, L. Yi, L. Zheng, W. Wang, H. X. Zhang, H. Zhang and J. Zhang, Angew. Chem. Int. Ed., 2021, **60**, 16687-16692.

(7) J. Kim, W. Choi, J. W. Park, C. Kim, M. Kim and H. Song, J. Am. Chem. Soc., 2019, **141**, 6986-6994.

(8) F. Li, A. Thevenon, A. Rosas-Hernandez, Z. Wang, Y. Li, C. M. Gabardo, A. Ozden, C. T. Dinh, J. Li, Y. Wang, J. P. Edwards, Y. Xu, C. McCallum, L. Tao, Z. Q. Liang, M. Luo, X. Wang, H. Li, C. P. O'Brien, C. S. Tan, D. H. Nam, R. Quintero-Bermudez, T. T. Zhuang, Y. C. Li, Z. Han, R. D. Britt, D. Sinton, T. Agapie, J. C. Peters and E. H. Sargent, Nature, 2020, **577**, 509-513.

(9) P. De Luna, R. Quintero-Bermudez, C.-T. Dinh, M. B. Ross, O. S. Bushuyev, P. Todorović, T. Regier, S. O. Kelley, P. Yang and E. H. Sargent, Nat. Catal., 2018, **1**, 103-110.

(10) D. Zhong, Z. J. Zhao, Q. Zhao, D. Cheng, B. Liu, G. Zhang, W. Deng, H. Dong, L. Zhang, J. Li, J. Li and J. Gong, Angew. Chem. Int. Ed., 2021, **60**, 4879-4885.

(11) W. Ma, S. Xie, T. Liu, Q. Fan, J. Ye, F. Sun, Z. Jiang, Q. Zhang, J. Cheng and Y. Wang, Nat. Catal., 2020, **3**, 478-487.

(12) X. Chen, J. Chen, N. M. Alghoraibi, D. A. Henckel, R. Zhang, U. O. Nwabara, K. E. Madsen, P. J. A. Kenis, S. C. Zimmerman and A. A. Gewirth, Nat. Catal., 2020, 4, 20-27.

(13) H. Li, T. Liu, P. Wei, L. Lin, D. Gao, G. Wang and X. Bao, Angew. Chem. Int. Ed., 2021, **60**, 14329-14333.

(14) M. Zheng, P. Wang, X. Zhi, K. Yang, Y. Jiao, J. Duan, Y. Zheng and S. Z. Qiao, J. Am. Chem. Soc., 2022, **144**, 14936-14944.
(15) C. T. Dinh, T. Burdyny, M. G. Kibria, A. Seifitokaldani, C. M. Gabardo, F. P. G. de Arquer, A. Kiani, J. P. Edwards, P. De Luna, O. S. Bushuyev, C. Q. Zou, R. Quintero-Bermudez, Y. J. Pang, D. Sinton and E. H. Sargent, Science, 2018, **360**, 783-787.
(16) F. P. G. de Arquer, C. T. Dinh, A. Ozden, J. Wicks, C. McCallum, A. R. Kirmani, D. H. Nam, C. Gabardo, A. Seifitokaldani, X. Wang, Y. G. C. Li, F. W. Li, J. Edwards, L. J. Richter, S. J. Thorpe, D. Sinton and E. H. Sargent, Science, 2020, **367**, 661-666.
(17) Y. Zhou, F. Che, M. Liu, C. Zou, Z. Liang, P. De Luna, H. Yuan, J. Li, Z. Wang, H. Xie, H. Li, P. Chen, E. Bladt, R. Quintero-Bermudez, T. K. Sham, S. Bals, J. Hofkens, D. Sinton, G. Chen and E. H. Sargent, Nat. Chem., 2018, **10**, 974-980.
(18) J. Y. Kim, G. Kim, H. Won, I. Gereige, W. B. Jung and H. T. Jung, Adv. Mater., 2022, **34**, e2106028.
(19) R. Feng, Q. Zhu, M. Chu, S. Jia, J. Zhai, H. Wu, P. Wu and B. Han, Green Chem., 2020, **22**, 7560-7565.
(20) M. Balamurugan, H. Y. Jeong, V. S. K. Choutipalli, J. S. Hong, H. Seo, N. Saravanan, J. H. Jang, K. G. Lee, Y. H. Lee, S. W. Im, V. Subramanian, S. H. Kim and K. T. Nam, Small, 2020, **16**, e2000955.
(21) S. Lee, G. Park and J. Lee, ACS Catal., 2017, **7**, 8594-8604.
(22) W. Liu, P. Zhai, A. Li, B. Wei, K. Si, Y. Wei, X. Wang, G. Zhu, Q. Chen, X. Gu, R. Zhang, W. Zhou and Y. Gong, Nat. Commun., 2022, 13, 1877.
(23) X. Zhang, J. Li, Y. Y. Li, Y. Jung, Y. Kuang, G. Zhu, Y. Liang and H. Dai, J. Am. Chem. Soc., 2021, **143**, 3245-3255.
(24) D. Ren, Y. Deng, A. D. Handoko, C. S. Chen, S. Malkhandi and B. S.Yeo, *ACS Catal.*, 2015, **5**, 2814-2821.
(25) Y. Song, R. Peng, D. K. Hensley, P. V. Bonnesen, L. Liang, Z. Wu, H. M. Meyer, M. Chi, C. Ma, B. G. Sumpter and A. J. Rondinone, *ChemistrySelect*, 2016, **1**, 6055-6061.
(26) D. Ren, B. S.-H. Ang and B. S. Yeo, *ACS Catal.*, 2016, **6**, 8239-8247.
(27) H. Mistry, A. S. Varela, C. S. Bonifacio, I. Zegkinoglou, I. Sinev, Y. W. Choi, K. Kisslinger, E. A. Stach, J. C. Yang, P. Strasser and B. R. Cuenya, *Nat. Commun.*, 2016, **7**, 12123.

(28) A. Loiudice, P. Lobaccaro, E. A. Kamali, T. Thao, B. H. Huang, J. W. Ager and R. Buonsanti, *Angew. Chem. Int. Ed.*, 2016, **55**, 5789-5792.

(29) C. G. Morales-Guio, E. R. Cave, S. A. Nitopi, J. T. Feaster, L. Wang, K. P. Kuhl, A. Jackson, N. C. Johnson, D. N. Abram, T. Hatsukade, C. Hahn and T. F. Jaramillo, *Nat. Catal.*, 2018, **1**, 764-771.

(30) K. Jiang, R. B. Sandberg, A. J. Akey, X. Liu, D. C. Bell, J. K. Nørskov, K. Chan and H. Wang, *Nat. Catal.*, 2018, **1**, 111-119.

(31) M. Ma, K. Djanashvili and W. A. Smith, Angew. Chem. Int. Ed., 2016, 55, 6680-6684.

(32) A. S. Varela, W. Ju, T. Reier and P. Strasser, *ACS Catal.*, 2016, **6**, 2136-2144.

(33) X. Wang, Z. Wang, F. P. García de Arquer, C.-T. Dinh, A. Ozden, Y. C. Li, D.-H. Nam, J. Li, Y.-S. Liu, J. Wicks, Z. Chen, M. Chi, B. Chen, Y. Wang, J. Tam, J. Y. Howe, A. Proppe, P. Todorović, F. Li, T.-T. Zhuang, C. M. Gabardo, A. R. Kirmani, C. McCallum, S.-F. Hung, Y. Lum, M. Luo, Y. Min, A. Xu, C. P. O'Brien, B. Stephen, B. Sun, A. H. Ip, L. J. Richter, S. O. Kelley, D. Sinton and E. H. Sargent, *Nat. Energy*, 2020, **5**, 478-486.

(34) T.-T. Zhuang, Z.-Q. Liang, A. Seifitokaldani, Y. Li, P. De Luna, T. Burdyny, F. Che, F. Meng, Y. Min, R. Quintero-Bermudez, C. T. Dinh, Y. Pang, M. Zhong, B. Zhang, J. Li, P.-N. Chen, X.-L. Zheng, H. Liang, W.-N. Ge, B.-J. Ye, D. Sinton, S.-H. Yu and E. H. Sargent, *Nat. Catal.*, 2018, **1**, 421-428.

(35) C. Peng, G. Luo, Z. Xu, S. Yan, J. Zhang, M. Chen, L. Qian, W. Wei, Q. Han and G. Zheng, *Adv. Mater.*, 2021, **33**, e2103150.

(36) S. Ma, M. Sadakiyo, R. Luo, M. Heima, M. Yamauchi and P. J. A. Kenis, *J. Power Sources*, 2016, **301**, 219-228.

(37) J. J. Lv, M. Jouny, W. Luc, W. Zhu, J. J. Zhu and F. Jiao, *Adv. Mater.*, 2018, **30**, e1803111.

(38) T. T. H. Hoang, S. Verma, S. Ma, T. T. Fister, J. Timoshenko, A. I. Frenkel, P. J. A. Kenis and A. A. Gewirth, *J. Am. Chem. Soc.*, 2018, **140**, 5791-5797.

(39) Y. Wang, Z. Wang, C.-T. Dinh, J. Li, A. Ozden, M. Golam Kibria, A. Seifitokaldani, C.-S. Tan, C. M. Gabardo, M. Luo, H. Zhou, F. Li, Y. Lum, C. McCallum, Y. Xu, M. Liu, A. Proppe, A. Johnston, P. Todorovic, T.-T. Zhuang, D. Sinton, S. O. Kelley and E. H. Sargent, *Nat. Catal.*, 2019, **3**, 98-106.

(40) L. Han, W. Zhou and C. Xiang, *ACS Energy Lett.*, 2018, **3**, 855-860.

(41) J. E. Huang, F. W. Li, A. Ozden, A. S. Rasouli, F. P. G. de Arquer, S. J. Liu, S. Z. Zhang, M. C. Luo, X. Wang, Y. W. Lum, Y. Xu, K. Bertens, R. K. Miao, C. T. Dinh, D. Sinton and E. H. Sargent, *Science*, 2021, **372**, 1074-1078.

(42) C. P. O'Brien, R. K. Miao, S. Liu, Y. Xu, G. Lee, A. Robb, J. E. Huang, K. Xie, K. Bertens, C. M. Gabardo, J. P. Edwards, C.-T. Dinh, E. H. Sargent and D. Sinton, ACS Energy Lett., 2021, **6**, 2952-2959.

(43) M. Krödel, B. M. Carter, D. Rall, J. Lohaus, M. Wessling and D. J. Miller, ACS Appl. Mate. Inter., 2020, **12**, 12030-12042.

(44) T.-y. Chen, J. Hu, K.-z. Wang, G.-y. Gan and J. Shi, Ionics, 2021, **27**, 3639-3645.

(45) A. Pătru, T. Binninger, B. Pribyl and T. J. Schmidt, J. Electrochem. Soc. 2019, **166**, F34-F43.

(46) R. K. Miao, Y. Xu, A. Ozden, A. Robb, C. P. O'Brien, C. M. Gabardo, G. Lee, J. P. Edwards, J. E. Huang, M. Fan, X. Wang, S. Liu, Y. Yan, E. H. Sargent and D. Sinton, Joule, 2021, **5**, 2742-2753.

(47) Y. Xu, F. Li, A. Xu, J. P. Edwards, S. F. Hung, C. M. Gabardo, C. P. O'Brien, S. Liu, X. Wang, Y. Li, J. Wicks, R. K. Miao, Y. Liu, J. Li, J. E. Huang, J. Abed, Y. Wang, E. H. Sargent and D. Sinton, Nat. Commun., 2021, **12**, 2932.

(48) Y. C. Li, G. Lee, T. Yuan, Y. Wang, D.-H. Nam, Z. Wang, F. P. García de Arquer, Y. Lum, C.-T. Dinh, O. Voznyy and E. H. Sargent, ACS Energy Lett., 2019, **4**, 1427-1431.

(49) Y. Xu, R. K. Miao, J. P. Edwards, S. Liu, C. P. O'Brien, C. M. Gabardo, M. Fan, J. E. Huang, A. Robb, E. H. Sargent and D. Sinton, Joule, 2022, **6**, 1333-1343.

(50) Y. Xu, J. P. Edwards, J. Zhong, C. P. O'Brien, C. M. Gabardo, C. McCallum, J. Li, C.-T. Dinh, E. H. Sargent and D. Sinton, Energ. Environ. Sci., 2020, **13**, 554-561.

(51) W. Zhu, S. Kattel, F. Jiao and J. G. Chen, Adv. Energy Mater., 2019, 9, 1802840.

(52) G. Wen, B. Ren, X. Wang, D. Luo, H. Dou, Y. Zheng, R. Gao, J. Gostick, A. Yu and Z. Chen, Nature Energy, 2022, 7, 978-988.

(53) W. Li, Z. Yin, Z. Gao, G. Wang, Z. Li, F. Wei, X. Wei, H. Peng, X. Hu, L. Xiao, J. Lu and L. Zhuang, Nature Energy, 2022, 7, 835-843.

(54) Y. Xu, R. K. Miao, J. P. Edwards, S. Liu, C. P. O'Brien, C. M. Gabardo, M. Fan, J. E. Huang, A. Robb, E. H. Sargent and D. Sinton, Joule, 2022, 6, 1-11.

(55) J. Gu, S. Liu, W. Ni, W. Ren, S. Haussener and X. Hu, Nat. Catal., 2022, **5**, 268-276.

(56) T. Zheng, K. Jiang, N. Ta, Y. Hu, J. Zeng, J. Liu and H. Wang, Joule, 2019, **3**, 265-278.